Design of a High Selectivity Filter for MRI Guided RF Hyperthermia Therapy

Please check the document version of this publication:

Design of a High Selectivity Filter for MRI Guided RF Hyperthermia Therapy

Kemal Sumser[1], Sander Bronckers[2], Marjolein Kleijer[2], Margarethus M. Paulides[1,2]

[1]Department of Radiotherapy, Erasmus M.C., Rotterdam, The Netherlands

[2]Department of Electrical Engineering, Eindhoven University of Technology, Eindhoven, The Netherlands

Abstract—**Hyperthermia devices have been integrated with MR scanners to exploit MR thermometry. Integrating two RF systems require the filtering of high-power RF heating signal from MR system for simultaneous heating and imaging. Currently, a filter that suppresses 100MHz and its harmonics is in use. Development of a MR-compatible hyperthermia applicator for head and neck requires a filter that can suppress also the 433.92MHz signal. A unique new filter which has high power handling, extremely high suppression, and selectivity has been designed that attenuates 100MHz and 433.92MHz signals with low insertion loss (<0.25dB) at 63.89MHz. 0.14dB insertion loss at 63.89MHz, 112dB, 88dB and 93dB signal attenuation were achieved at 100MHz, 200MHz and 433.92MHz, respectively, with the new filter design using model of LM-500 cable. A proof of concept filter was constructed to validate the design. Our investigation shows that filter requirements can be satisfied, but high-power low-loss coaxial cables are necessary.**

Index Terms—**Hyperthermia, MRI, MR Image Quality, filters, MRT.**

I. INTRODUCTION

Hyperthermia treatments are aim to increase the target tissue temperature to 40-44 °C for 30-60 minutes [1]. These temperatures are most commonly achieved by applying focused electromagnetic radiation at radio frequencies [2]. Clinical studies have shown that the effects of chemotherapy and radiotherapy are enhanced by applying a sufficient thermal dose [3, 4]. Due to patient specific thermoregulation, temperature monitoring is essential to monitor and adapt the thermal dose. Only magnetic resonance thermometry can provide sufficiently accurate noninvasive 3D temperature monitoring in the clinic. This prompts the development of radiofrequency hyperthermia applicators compatible with MR scanners [5]. Since MR imaging is also operates at radio frequencies, the high-power signals from the hyperthermia applicators must be decoupled from the MR scanner.

The most common option to integrate a hyperthermia system with MR imaging is by decoupled inserts [5]. These devices operate with an RF transmission (TX) chain that is independent from the MR scanner's RF TX/RX chain,

therefore heating and imaging can be performed simultaneously. For truly simultaneous operation, the heating RF signal needs to be filtered out from the imaging RX signal for two reasons. First, the heating signal carries high-power RF waves that can damage the MR scanner's hardware. Second, the interaction between the heating signal and the MR RX can distort the imaging. Therefore, a filter is needed to solve the interference between the MRI scanner and the hyperthermia applicator.

Currently, a hyperthermia applicator, operating at 100 MHz, and a 1.5 T MRI, operating at 63.89 MHz, are used for MRI-guided deep pelvis hyperthermia at Erasmus MC [6]. There exists a filter, which is implemented in the MRI scanner, that attenuates the signal of this 100 MHz hyperthermia applicator [7]. However, a new hyperthermia applicator, operating at 433.92 MHz, has been designed at Erasmus MC that will be used for MRI-guided deep head and neck hyperthermia treatments. A new filter that also attenuates the 433.92 MHz signal is needed before this applicator can be used in practice. This unique filter design requires high power handling capabilities, low insertion losses at MRI Larmor frequency and high suppression and selectivity at three distinct frequencies. This concept has been illustrated in Figure 1.

In this paper, new filter design options that allows simultaneous MR imaging at 1.5 T and RF hyperthermia at 100 MHz and 433.92 MHz are investigated. First, the requirements for the filter and the currently installed filter in the MRI system has been described. Then two new filter architectures are introduced, as well as different coaxial cables that can be used in the design. Next, the new filter designs are intercompared and the best performing design architecture chosen for experimental testing. A proof of concept is described and the results of this proof of concept are discussed.

II. REQUIREMENTS

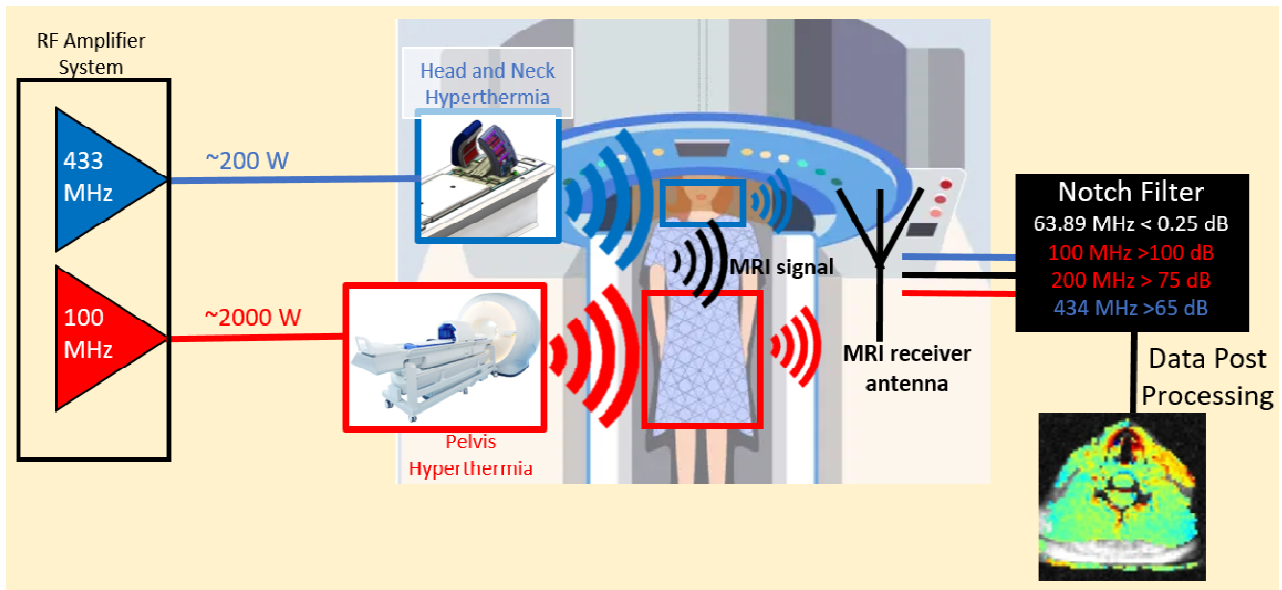For the clinical setup, two different types of hyperthermia

Figure 1. Scheme of the overall system for MRI guided hyperthermia, with hyperthermia applicators inside the MRI that contains the body coil. The systems are decoupled by filtering the high-power heating signals (200-2000 W) from the signals received by the body (1-2 µW), before they are processed further.

systems are considered. First, a deep pelvis hyperthermia system that has an operating frequency of 100 MHz with an operating power of 1-2 kW. Second, a deep head and neck hyperthermia system that has an operating frequency of 433.92 MHz with an operating power of 200 W. The MRI receive system that needs to be very sensitive for very low signal returning from the body operates at 1-2 µW. The clinical setup is supposed to operate for both hyperthermia systems without changing any other components in the setup. This means that a single filter needs to be designed that operates for both hyperthermia devices. MR data acquisition is performed using a 1.5 Tesla MRI that operates at 63.89 MHz.

In Table 1, the filter requirements and the characteristics of the current filter are given. The insertion loss of the 1.5 Tesla MRI signal at 63.89 MHz should be less than 0.25 dB. The 100 MHz component needs to be suppressed by at least 100 dB such that it does not damage the MRI amplifiers. For the second harmonic of the 100 MHz signal, at 200 MHz, is assumed that it should be suppressed by at least 75 dB [7]. Sumser et al. [8] reported -55 dB decoupling with MRI surface receiver coils and 433.92 MHz phased array system. Therefore, the 433.92 MHz component needs to be suppressed by at least 65 dB.

Table 1. Filter requirements and the characteristics of the current filter

Attenuation at	Requirement	Current Design
63.89 MHz	< 0.25 dB	0.26 dB
100 MHz	> 100 dB	78 dB
200 MHz	> 75 dB	62 dB
433 MHz	> 65 dB	3.7 dB

The current filter is schematically shown in Figure 2. Coaxial lines are used for this filter to enable high power handling and to prevent radiation into the MRI. The filter consists of two pairs of stubs to attenuate the signal at 100 MHz and at the second harmonic of 100 MHz, at 200 MHz. Cable 5 that separates the pairs of stubs assures maximum power transfer at 63.89 MHz. The current filter, designed only to be used with the BSD2000 3D MRI system, does not meet the filter requirements. For the current filter, the measured attenuation at 63.89 MHz is 0.26 dB, while the measured attenuations at 100 MHz and 200 MHz are 22 dB and 13 dB too low than the requirements, respectively. The filter does not significantly attenuate the signal at 433.92 MHz. Even though the measurement results do not meet the given requirements, these filters are currently used in the MRI scanner. This suggests that the stated requirements might be more strict than required due to the assumptions made in the estimation of requirements.
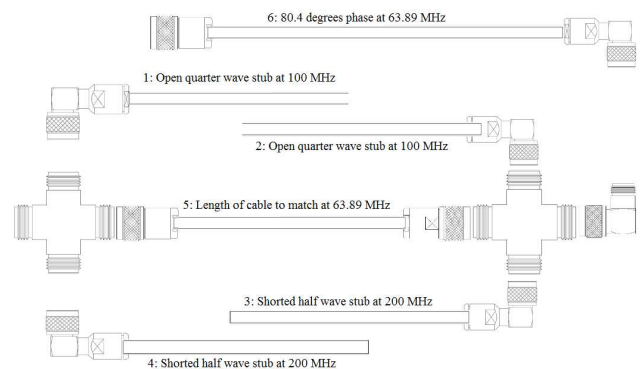

Figure 2. Schematic of the current BSD Medical 100MHz hyperthermia filter

III. NEW FILTER DESIGNS

The filters were designed and simulated using PathWave Advanced Design System (ADS) software by Keysight Technologies. The coax parameters in ADS are set using the data from the datasheet and the dielectric properties of the cable. The parameters responsible for the attenuation are set by tuning a 100 ft length of coaxial cable to approximate the given attenuations at their corresponding frequencies.

A. Improved Filter Design 1

The most significant shortcoming of the current filter design is that, it does not attenuate the 433.92 MHz signal. Therefore, first, the current design has been improved to satisfy the requirements set for 433.92 MHz signal. Cable 6 of the current filter, shown in Figure 2, is removed in the new designs, since it does not significantly influence the transmission response of the filter. An additional pair of shorted half wave stubs at 433.92 MHz has been added to the design at the same place as the current stubs. A schematic of the Improved Filter Design 1 (IFD1) is shown in Figure 3.

B. Improved Filter Design 2

The current filter design (while it provides a satisfactory operation) does not fulfill the requirements at 100 MHz. To improve the attenuation at 100 MHz, also an extra pair of stubs for 100 MHz is added to IFD1, which results in Improved Filter Design 2 (IFD2), shown in Figure 4.

C. Coaxial Cable Choice

The insertion loss at 63.89 MHz for the current filter design is at the limit and additional stubs will create more insertion losses. These insertion losses should be reduced. A possible way to improve this aspect is through the usage of a coaxial cable that has a low power dissipation which can be found on a cable's datasheet at attenuation per 100 feet. The type of coaxial cable that has been used for the current filter is RG-393. The filter designs are simulated with two other coaxial cables that have lower power dissipation characteristics than RG-393: LMR-1700 and LMR-500. These are compared to RG-393 cables.

IV. RESULTS

The obtained results for new filter designs and different coaxial cable choices are given in Table 2. IFR1 with RG-393 coaxial cable satisfies the requirements set for 433.92 MHz. However, it is unable to meet the requirements for the insertion loss at 63.89 MHz and the attenuation at 100 MHz. While changing the coaxial cable to LM-500 satisfied the requirements for the insertion loss, this design still is not satisfactory to attenuate the 100 MHz signal. However, the filter design fulfilled all requirements when the LM-1700 cable was substituted.

IFR2 with RG-393 was able to fulfill all requirements set for the signal rejection. However, the insertion loss at 63.89 MHz is too high for satisfactory MRI application. the filter meets the requirement at 100 MHz, 200 MHz and 433.92 MHz and approaches the requirement at 63.89 MHz as good as possible. Therefore it can be concluded, that this is the most suitable design from the three designs considered. Substituting the RG-393 cable with either a LM-500 or LM-1700 enables fulfillment of also the last requirement set.

V. PROOF OF CONCEPT

A proof the concept of the new design, IFR2, a prototype was fabricated using a URM-76 cable and measured. Since this cable type has different parameters and higher attenuation values than the RG-393 cable, we expect worse performance than the RG-393 cable, but still sufficient to validate the design architecture. A simulation of the new
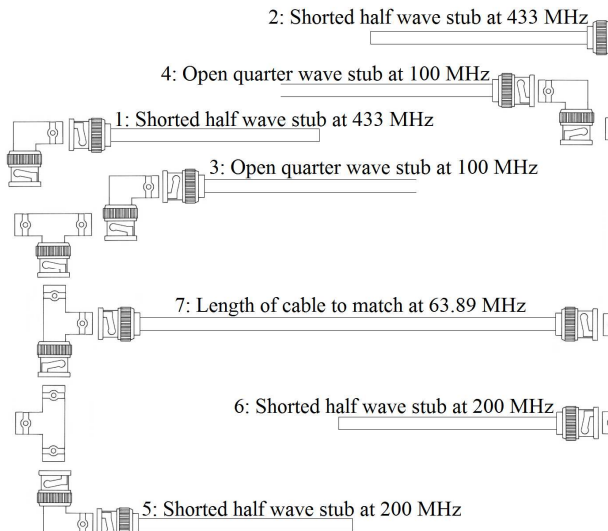

Figure 3. Schematic design of Improved Filter Design 1. The filter consists of three pairs of stubs (cable 1-6), to suppress the signal at 100 MHz, 200 MHz and 433 MHz. The length of cable that separates the pairs of stubs (cable 7) assures maximum power transfer at 63.89 MHz.
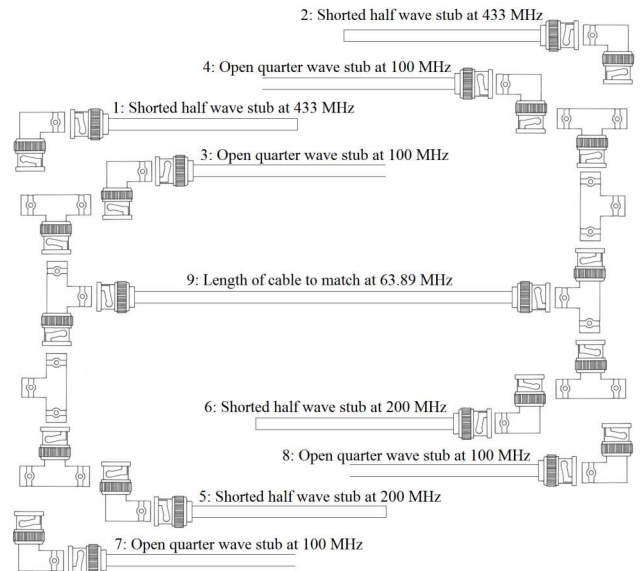

Figure 4. Schematic design of Improved Filter Design 2. The filter consists of three pairs of stubs (cable 1-6), to suppress the signal at 100 MHz, 200 MHz and 433 MHz. The length of cable that separates the pairs of stubs (cable 7) assures maximum power transfer at 63.89 MHz.

Table 2. Attenuation characteristics for the current filter and IFR1 and IFR2 for three different cables. The results that fulfilled the requirements are color-coded in green and the results that do not meet the requirements color-coded in orange.

Attenuation at	Requirement	Current Filter	IFR1			IFR2		
		RG-393	RG-393	LM-500	LM-1700	RG-393	LM-500	LM-1700
63.89 MHz	< 0.25 dB	0.26 dB	0.28 dB	0.12 dB	0.03 dB	0.33 dB	0.14 dB	0.04 dB
100 MHz	> 100 dB	78 dB	58.6	81.2	103 dB	100 dB	112 dB	146 dB
200 MHz	> 75 dB	62 dB	64.4	75.6	99 dB	79 dB	88 dB	112 dB
433 MHz	> 65 dB	3.7 dB	84.3	92.1	117 dB	69 dB	93 dB	114 dB

design with the parameters of the URM-76 cable was also performed.

A. Simulations

The results of the simulated transmission of the design is shown in Figure 4. The values of the attenuation at 63.89 MHz, 100 MHz, 200 MHz and 433.92 MHz are 0.56 dB, 89 dB, 67 dB and 71 dB, respectively. These results confirm that this design can satisfy the requirements for 200 MHz and 434 MHz, but requires better cables to fulfill the requirements at 63.89 MHz and 100 MHz.

B. Prototype

First, the stub cables are cut to approximately the length used in the simulation. However, the adapters in the simulation are lossless, so extra length is added by the adapters in practice. The stubs were individually iteratively tuned to a smaller length to compensate for the adapters and simulation errors to get the optimal stub length.

C. Measurements

The S-parameters of the prototype were measured with a network vector analyzer (ZNC 3, Rhode & Schwarz, Germany). The result of the measurement is shown in Figure 5. The values of the attenuation at 63.89 MHz, 100 MHz, 200 MHz and 433.92 MHz are 0.84 dB, 89 dB, 60 dB and 42 dB, respectively. The shape of the measurement is similar to the shape of the simulation up to ~250 MHz, but deviates more at higher frequencies. This might be caused by the fact that a small change in a certain stub length has a larger effect at higher than at lower frequencies. The measured attenuation of the dip around 400 MHz is less and the measured attenuation of the peak right to this dip is more than in the simulation. This could be caused by the larger frequency shift in the dip around 400 MHz, which brings this dip and the peak at the right from this dip closer together. Finally, it is shown that the insertion loss at 63.89 MHz is 0.28 dB higher in practice than in the simulation. This extra loss is probably caused by the connectors and adapters, which were lossless in the simulation.

VI. DISCUSSION & CONCLUSIONS

From the comparison between the results of the proof of concept, the results of the simulations of the improved filter in RG-393 cable and the results of the current filter, it can be concluded that IFR2 will work better than the current filter at

100 MHz, 200 MHz and 433.92 MHz. The 0 dB and 7 dB difference between the simulation and measurement of the prototype, at 100 MHz and 200 MHz respectively, compared to the simulation of the improved design in the RG-393 cable, shows that, in practice, the attenuations for the improved filter at 100 MHz and 200 MHz will be higher than for the current filter. However, the results also show that the insertion loss at 63.89 MHz will be higher for the improved filter in comparison with the current filter. However, these downsides can be overcome by using cables with lower power dissipation characteristics, such as LM-500. In another note, the shape of the measurement of the prototype is not similar to the simulation of the prototype at frequencies higher than 250 MHz. The simulation and manufacturing process of the filter should be improved to make sure that the match between the measurement and simulation improves and a reliable conclusion can be drawn about the possible attenuation at 433.92 MHz. To fabricate the prototype with a higher precision would require more precise tools than currently available for the fabrication of the prototype.

VII. CONCLUSION

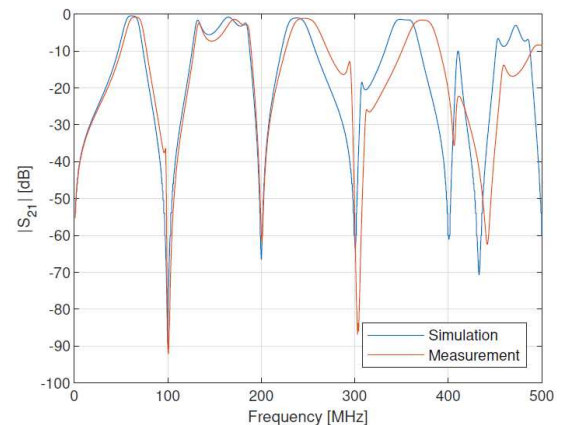The new filter enables signal shielding also at 433.92MHz. The simulation or design process of the

Figure 5. Simulated and measured magnitude of the transmission of the prototype of IFR2 with URM-76 cable. The shape of the measurement is similar to the shape of the simulation up to approximately 250 MHz, but is less similar at higher frequencies

prototype should be improved to improve the similarity between the simulation and the measurement and enable simulation based optimization.

VIII. ACKNOWLEDGEMENTS

REFERENCES

1. Kok, H.P., et al., *Heating technology for malignant tumors: a review.* International Journal of Hyperthermia, 2020. **37**(1): p. 711-741.
2. Paulides, M.M., et al., *Recent technological advancements in radiofrequency-and microwave-mediated hyperthermia for enhancing drug delivery.* Advanced Drug Delivery Reviews, 2020.
3. Franckena, M., et al., *Hyperthermia dose-effect relationship in 420 patients with cervical cancer treated with combined radiotherapy and hyperthermia.* European Journal of Cancer, 2009. **45**(11): p. 1969-1978.
4. Kroesen, M., et al., *Confirmation of thermal dose as a predictor of local control in cervical carcinoma patients treated with state-of-the-art radiation therapy and hyperthermia.* Radiotherapy and Oncology, 2019. **140**: p. 150-158.
5. Adibzadeh, F., et al., *Systematic review of pre-clinical and clinical devices for magnetic resonance-guided radiofrequency hyperthermia.* International Journal of Hyperthermia, 2020. **37**(1): p. 15-27.
6. Mulder, H.T., et al., *Systematic quality assurance of the BSD2000-3D MR-compatible hyperthermia applicator performance using MR temperature imaging.* International Journal of Hyperthermia, 2018. **35**(1): p. 305-313.
7. Gellermann, J., et al., *A practical approach to thermography in a hyperthermia/magnetic resonance hybrid system: Validation in a heterogeneous phantom.* International Journal of Radiation Oncology* Biology* Physics, 2005. **61**(1): p. 267-277.
8. Sumser, K., et al., *Dual-Function MR-guided Hyperthermia: An Innovative Integrated Approach and Experimental Demonstration of Proof of Principle.* IEEE Transactions on Biomedical Engineering, 2020.